REPORT DOCUMENTATION PAGE

Public reporting burden for this collection of information is estimated to average 1 hour per response, including the time for reviewing instructions, searching existing data sources, gathering and maintaining the data needed, and completing and reviewing the collection of information. Send comment regarding this burden estimates or any other aspect of this collection of information, including suggestions for reducing this burden, to Washington Headquarters Services, Directorate for information Operations and Reports, 1215 Jefferson Davis Highway, Suite 1204, Arlington, VA 22202-4302, and to the Office of Management and Budget, Paperwork Reduction Project (0704-0188), Washington, DC 20503.

1. AGENCY USE ONLY *(Leave blank)*	2. REPORT DATE 30 September 1996	3. REPORT TYPE AND DATES COVERED Final Report: 9/28/94 to 9/27/96

4. TITLE AND SUBTITLE
A Pore Structure Model for Coupling Subscale
Reactions to the Macroscopic Transport

5. FUNDING NUMBERS

DAAH04-94-C-0075

6. AUTHOR(S)

Girard A. Simons

7. PERFORMING ORGANIZATION NAMES(S) AND ADDRESS(ES)

Simons Research Associates
3 Juniper Road
Lynnfield, MA 01940-2416

8. PERFORMING ORGANIZATION REPORT NUMBER

9. SPONSORING / MONITORING AGENCY NAME(S) AND ADDRESS(ES)

U.S. Army Research Office
P.O. Box 12211
Research Triangle Park, NC 27709-2211

10. SPONSORING / MONITORING AGENCY REPORT NUMBER

ARO 32900.6-GS-S

11. SUPPLEMENTARY NOTES

The views, opinions and/or findings contained in this report are those of the author(s) and should not be construed as an official Department of the Army position, policy or decision, unless so designated by other documentation.

12a. DISTRIBUTION / AVAILABILITY STATEMENT

Approved for public release; distribution unlimited.

19961025 083

13. ABSTRACT *(Maximum 200 words)*

The "pore tree" model of pore structure (Simons and Finson, 1979; Simons, 1982) was developed for catalyst and sorbent grains to allow coupled diffusion and chemical reactions within porous media in the absence of convection through the media. The pore tree model has been extended to describe the permeable pore structure which characterizes the subsurface flow of gas and water in soil. The description of permeability required a statistical determination of the "branches" that are common to several trees to allow percolation through the large scale (mobile) structure in addition to diffusion through the smaller scale (immobile) structure. Subsequently, the pore tree model has been adapted to describe hydrodynamic dispersion which represents a preliminary step in the description of the subscale convection necessary to relate macroscopic transport, subscale diffusion and chemical reactions. A methodology has been developed to couple subscale convection, diffusion and chemical reactions to the macroscopic transport in order to accurately describe contaminant transport and in-situ remediation in Ground Water Simulation codes.

DTIC QUALITY INSPECTED 1

14. SUBJECT TERMS

Pore Structure, Permeability, Hydrodynamic Dispersion, Subscale Reactions

15. NUMBER OF PAGES
38

16. PRICE CODE

17. SECURITY CLASSIFICATION OR REPORT	18. SECURITY CLASSIFICATION OF THIS PAGE	19. SECURITY CLASSIFICATION OF ABSTRACT	20. LIMITATION OF ABSTRACT
UNCLASSIFIED	UNCLASSIFIED	UNCLASSIFIED	UL

A PORE STRUCTURE MODEL FOR COUPLING SUBSCALE REACTIONS TO THE MACROSCOPIC TRANSPORT

Final Report

Girard A. Simons

30 September 1996

Simons Research Associates
3 Juniper Road
Lynnfield, MA 01940-2416

THE VIEWS, OPINIONS, AND/OR FINDINGS CONTAINED IN THIS REPORT ARE
THOSE OF THE AUTHOR AND SHOULD NOT BE CONSTRUED AS AN OFFICIAL
DEPARTMENT OF THE ARMY POSITION, POLICY, OR DECISION, UNLESS SO
DESIGNATED BY OTHER DOCUMENTATION.

TABLE OF CONTENTS

I. INTRODUCTION AND SUMMARY OF THE RESEARCH PROGRAM

To properly describe coupled chemical reactions and gaseous diffusion in porous sorbent and catalyst grains, the "pore tree" was introduced by Simons and Finson (1979) and Simons (1982). The pore tree represents an isolated sub-structure, allowing diffusion into and out of porous media without permitting transport through the media. A pore size distribution was derived statistically and confirmed empirically for coal, coal char, sorbents, catalysts and kidney stones from both men and women. The pore tree was derived from the pore size distribution and allows 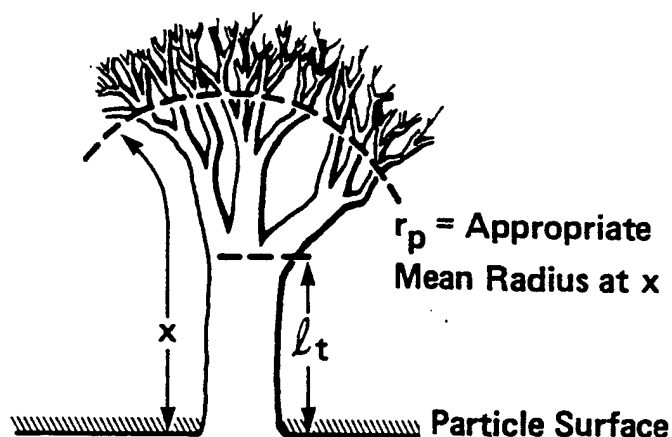the orderly migration of a reactant gas from the large pores to the small pores (Fig. 1). A detailed description of the pore tree and the coupled transport and chemistry is given by Simons (1982, 1983a). The spatially dependent transport/reaction equations are solved for a single pore tree and then the total contribution of all trees (of all sizes) in the system is obtained by summing the contribution of each tree that reaches the exterior of the system. This is distinct from the "bulk" transport approach in which the transport equation for a single pore is integrated over all pores at a fixed point in space before integrating spatially. The "bulk" transport approach is invalid if the spatial gradients in the transport equations are implicit functions of pore size. One example of this implicit pore size dependence is that of the heterogeneous reactions within porous sorbents (Simons, 1988) and catalysts for which the pore tree structure/transport model was developed. A second example is that of coupled diffusion and remediation reactions in the immobile region of soil.

r_p = Appropriate Mean Radius at x

Particle Surface

Figure 1. The Pore Tree

In order to describe the subsurface transport of gas and water in soil, the dispersion of contaminants, and in-situ remediation of contaminated sites, the pore tree has been extended (Simons, 1996a) to simulate permeability and bulk transport. The interconnectivity of the pore structure is illustrated in Fig. 2 and is obtained via a statistical determination of the "branches" that are common to several trees to allow convection and bulk diffusion through the large scale (mobile) structure in addition to diffusion and coupled chemical reactions within the smaller scale (immobile) structure. The statistical analysis has determined that the probability of pore interconnectivity extends across the entire pore size range, with an increase in the probability accompanying a decreasing pore size. While permeability is dominated by the largest pores, it is also important to establish the level of convection and diffusion that is occurring at the intermediate scales in order to accurately relate large scale bulk transport, small scale diffusion and coupled chemical reactions.
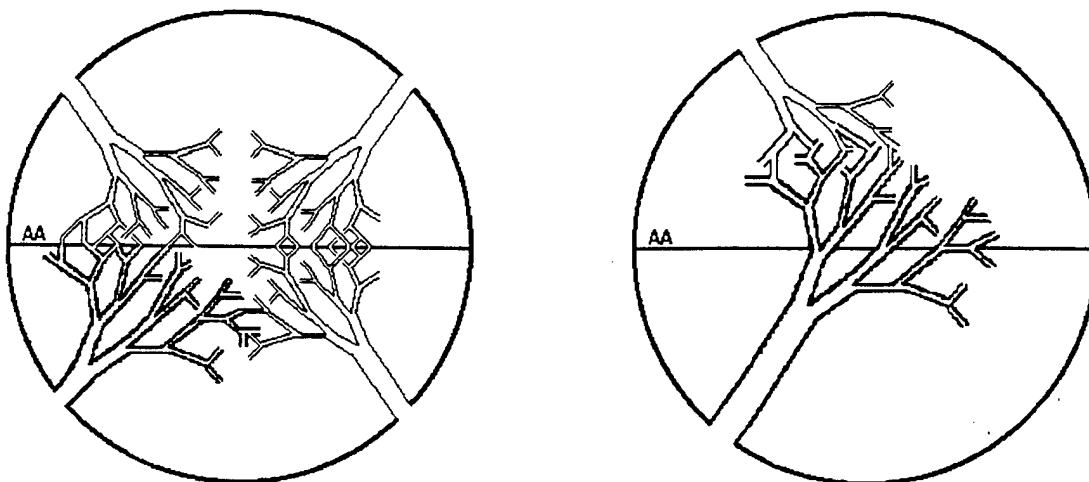
a) Pores Interconnected in Plane AA   b) Pores Interconnected Out of Plane AA

Figure 2. Interconnectivity of the Pore Tree

The permeability across a given plane is limited by the largest pores that are interconnected in that plane (Fig. 2a). The statistical analysis has determined that approximately one quarter of one percent of all large pores are interconnected. This establishes a very coarse grid for the permeability which leads to the measurement scale size errors illustrated in Fig. 3. The extended pore tree model has successfully explained the measurement errors in the permeability of soil due to the measurement scale size (Shouse, et.al., 1994) which has indirectly confirmed the low probability of the interconnectivity.

The bulk gaseous diffusivity across a given plane is shown to be limited by the interconnectivity of the smaller branches outside of that plane (Fig. 2b). These small pores may be saturated and gas diffusion is allowed only in pores whose radius is greater than that of the largest saturated pore (r_{sat}). The gas diffusivity is shown to

Figure 3. Measurement Scale Errors

scale as (permeability)$^{1/2}$/ r_{sat}. A comparison of the present theory to the diffusivity data of Washington et. al., (1994) is illustrated in Fig. 4. The gas diffusivity data at approximately 60% saturation verifies the permeability dependence and suggests a saturation radius of the order of 30 µm. Sixty percent saturation at 30 µm is consistent with the statistically derived
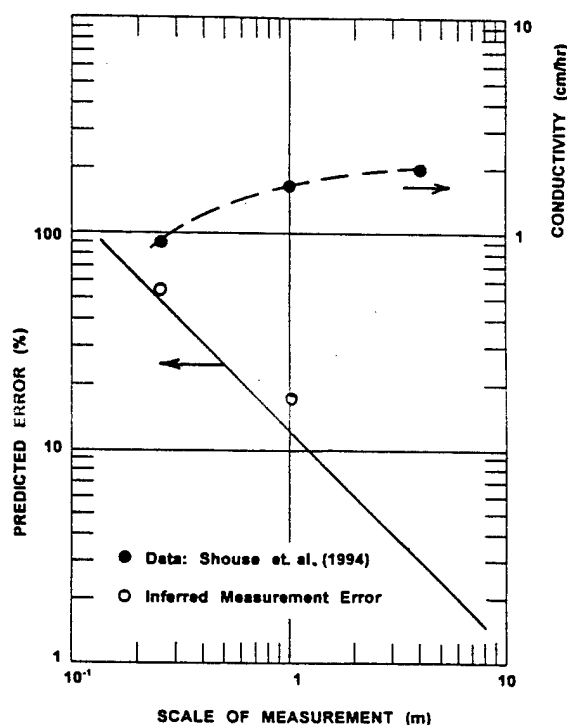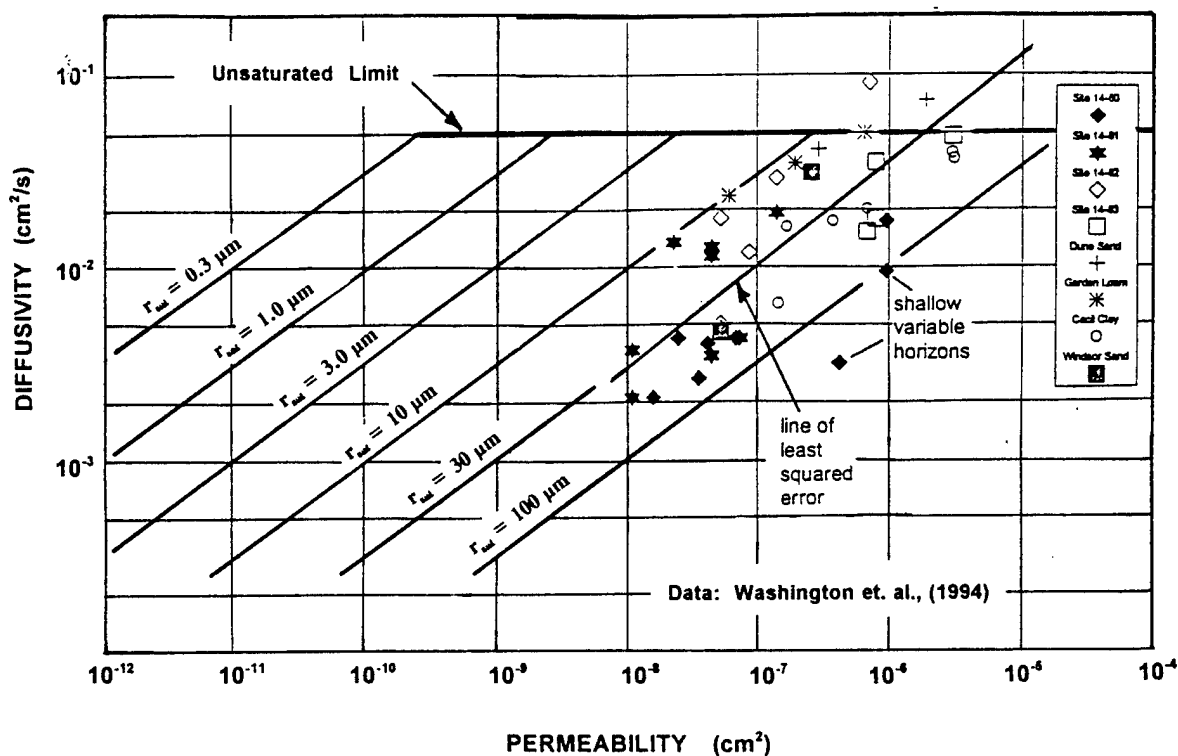
2

Figure 4. Bulk Diffusivity of a Partially Saturated Soil

pore size distribution function. While the excellent agreement with the data does substantiate the present theory, the diffusivity in partially saturated soil is very sensitive to an unknown saturation radius. If bulk diffusivities are to be correlated with field data, such measurements should attempt to measure the saturation radius.

The permeability and the bulk diffusivity have tested two extreme limits of the pore structure and pore interconnectivity concepts. Permeability is limited by the in plane interconnectivity (Fig. 2a) and bulk gaseous diffusion is limited by the out of plane (Fig. 2b) interconnectivity. Permeability is limited by the large pore interconnectivity and bulk diffusion is limited by the interconnectivity of the smaller pores. The apparent success of these concepts over a very broad pore size range suggests that the extended pore tree model will accurately describe the relationship between large scale convection and small scale diffusive transport.

A preliminary step in this approach to relate convective and diffusive transport in various size pores is to describe the subscale convection responsible for hydrodynamic dispersion (Simons, 1996b). The velocity profile in interconnected pore space is illustrated in Fig. 5. The largest pores are not interconneced across the porous medium. Hence, the net velocity within the largest pores is zero. The smallest pores do not support a very large convective velocity. Thus, there is a relative maximum of the velocity at some intermediate pore size $r_{max}/\sqrt{e}$. Clearly, the fluid in the pore of radius $r_{max}/\sqrt{e}$ convects ahead of that in the pores of radius r_1 and r_2. Consider flow in a saturated porous medium in which all fluid
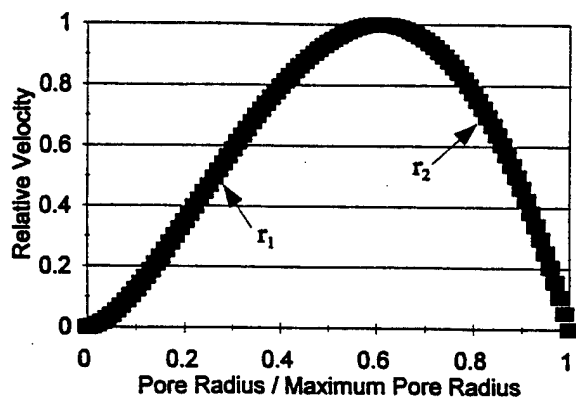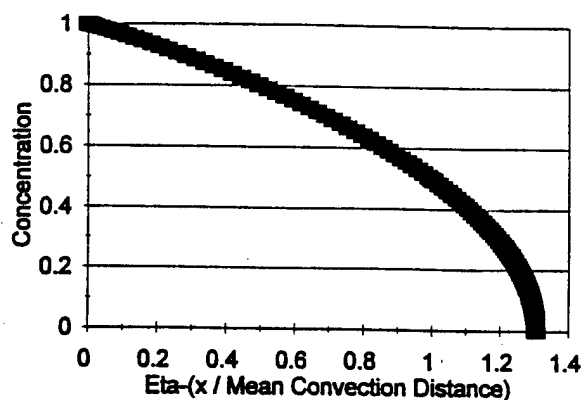
3

Figure 5. Velocity in Pore Space

Figure 6. Spatial Concentration Profile
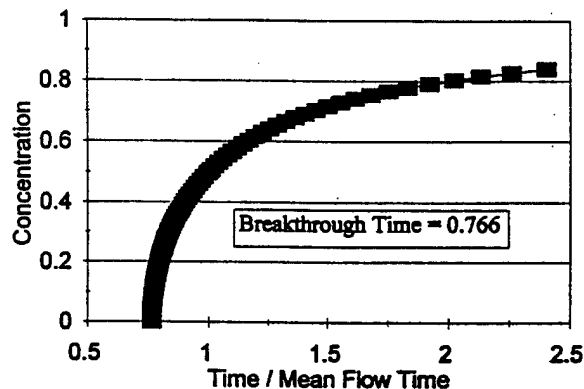
Figure 7. Temporal Concentration Profile
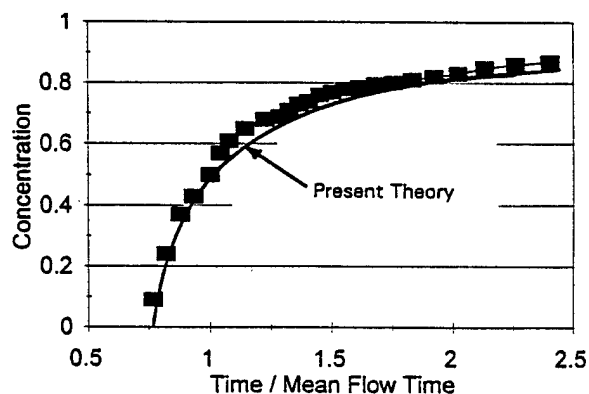
Figure 8. Temporal Concentration Data

behind a fixed plane normal to the flow is suddenly injected with red dye. If fluid velocity v_m^* is associated with pores r_1^* and r_2^*, all dyed fluid in pores whose radius is between r_1^* and r_2^* will translate with velocity equal to or greater than v_m^* and move to a corresponding location x^* or greater. The corresponding concentration profile is illustrated in Fig. 6 where all red dye would have reached the location Eta = 1 were it not for the velocity variation within pore size. The "front" of the concentration profile has progressed 30% ahead of the mean while the slower fluid in the smaller pores has trailed considerable. If we were standing at the end of a porous flow tube, the concentration passing our location would exhibit a time dependence illustrated in Fig. 7. The faster fluid breaks through ahead of the mean flow while the fluid in the smaller pores is delayed.

Data of Elrich, et al., (1966), as reported by Brusseau and Rao (1989), are illustrated in Fig. 8 and support the current theory of hydrodynamic dispersion. While the long "tail" of the concentration profile is generally attributed to nonequilibrium, the current pore structure

4

model attributes it to the wide pore size distribution occurring in soil. The narrow pore size distributions occurring in laboratory "soil" will yield a much narrower concentration profile, i.e., less hydrodynamic dispersion. Future research will be directed toward 1), evaluating the hydrodynamic dispersion as a function of pore size range in the soil sample and 2), using this analytic pore structure/ pore transport model to help derive an analytic expression for hydrodynamic dispersion that replaces the Fickian process in the transport equations.

Analysis of the permeability, bulk diffusivity, and hydrodynamic dispersion has utilized the interconnectivity of the pores to determine the distribution of the convection velocity with pore size. This analysis suggests the existence of a permeable sub-range in the pore structure which does not contribute significantly to the bulk permeability but in which convection dominates diffusion. It is the balance of the sub-scale convection with the small scale diffusion that will control contaminant transport and in-situ remediation. The size distribution of the pores and grains, and the variations in fluid velocity within and between pores of different sizes is critical to interfacing the transport processes. A methodology has been developed to couple subscale diffusion, convection and chemical reactions to the macroscopic transport in order to accurately describe contaminant transport and in-situ remediation in Ground Water Simulation codes.

A typical species transport equation in permeable soil is of the form:

$$\frac{\partial c}{\partial t} + \bar{v}\frac{\partial c}{\partial x} = D_h \frac{\partial^2 c}{\partial x^2} + \frac{c\dot{M}}{M}$$

where c is the local species concentration, $\bar{v}$ is the mean convection velocity as determined by the local pressure gradient and permeability k, and D_h is the hydrodynamic dispersion. The $\partial c/\partial t$ term is the true unsteady term and the source and/or sink of species c due to chemical and/or physical processes within the subscale pore structure is written as $c\dot{M}/M$ where $\dot{M}/M$ represents a bulk rate (1/t) of production or consumption. The bulk rate $\dot{M}/M$ will be related to gradients of c on length scales of order millimeters within the subscale pore structure and cannot be expressed in terms of the $\partial c/\partial x$ of the macroscopic transport grid.

To describe the subscale chemical reactions and transport, a "grain" of soil of radius a_g is isolated from the rest of the medium. The grain size will be chosen sufficiently small that diffusion and coupled chemical reactions will dominate the subscale transport. The pore tree was developed (Simons, 1982, 1983a,) to treat coupled chemical reactions and diffusion within immobile porous grains. Generic forms of the immobile solution are illustrated in Figure 9 where $\dot{R}_1$ represents the limit of kinetic control and $\dot{R}_2$ represents a coupled kinetic/diffusive solution in which the reaction on the walls of the pore establishes a species gradient which accelerates the molecular diffusion. The particular solution for contaminant transport and soil remediation will vary with the number of reactions and kinetic mechanisms but the generic form of the immobile solution will be similar to that illustrated in Fig. 9.

5
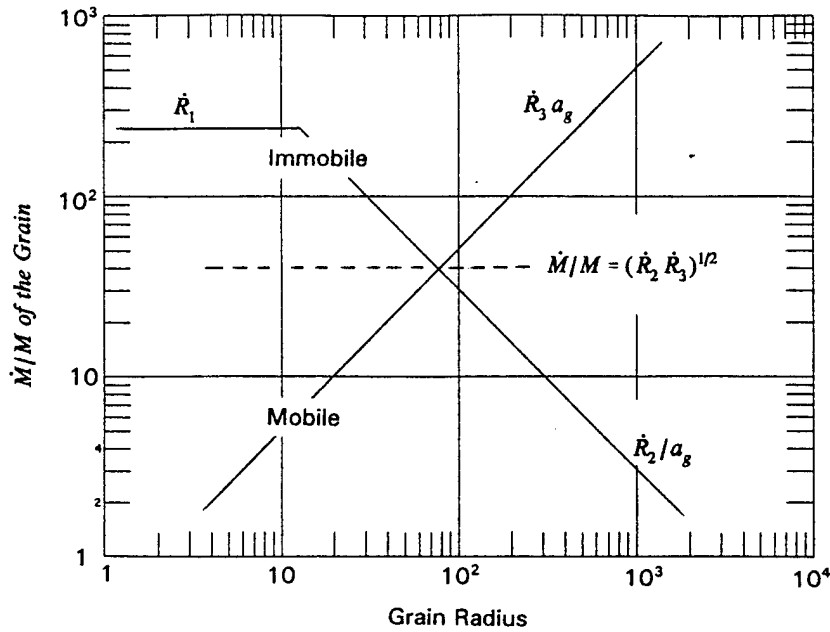
Figure 9. Coupling The Mobile and Immobile Solutions

The reactant species must be supplied to the edge of the grain by subscale convection at a rate depicted by the permeability which is appropriate to the length scale a_g. The mobile solution for $\dot{M}/M$ is developed in subsequent sections. It is shown that

$$\frac{\dot{M}}{M} = \frac{\theta^{5/3}\,(-dp/dx)}{768\,\mu\,\beta\,K_o^2}\,a_g \equiv \dot{R}_3\,a_g \quad (\textit{Convective Limit})$$

The mobile solution indicates that the convective limit increases with grain size while the immobile solution indicates that the diffusive limit decreases with increasing grain size. The comparison illustrated in Figure 9 suggests that for large grains, diffusion cannot keep up with convection while for small grains, convection cannot keep up with diffusion. The convective and diffusive limits are in balance if and only if

$$\frac{\dot{M}}{M} = \textit{Smaller Of } [\,(\dot{R}_2\,\dot{R}_3)^{1/2}\,,\ \dot{R}_1\,]$$

where it has been noted that the solution cannot exceed the limit of kinetic control.

The above expression for the bulk source and/or sink of species c due to chemical and/or physical processes within the subscale pore structure is incomplete without specific models for $\dot{R}_1$ and $\dot{R}_2$ in the immobile region. Future research will be directed toward developing a library of such models. The most basic processes of contaminant diffusion and adsorption are briefly described below.

6

II. ISOLATED PORE TREE: THE STRUCTURE

Following the pore structure theory of Simons and Finson (1979) and Simons (1982), consider a spherical porous particle of radius a, containing pores of length l_p and radius r_p. The pore dimensions range from a microscale of the order of Ångstroms to a macroscale which is a significant fraction of the particle radius. The radius of the largest pore is denoted by r_{max} and is given by

$$r_{max} = 2a\,\theta^{1/3}/3K_o \qquad (1)$$

where θ is the total porosity of the particle and K_o is a constant of integration, approximately equal to five, which relates the pore length to its radius

$$l_p = K_o\,r_p/\theta^{1/3} \qquad (2)$$

The radius of the smallest pore is denoted by r_{min} and is given by

$$r_{min} = 2\theta/\beta\,\rho_s s_p \qquad (3)$$

where ρ_s is the density of the solid matrix, s_p is the specific internal surface area (several hundred m²/g), and

$$\beta = \ln(r_{max}/r_{min}) \qquad (4)$$

The particle contains a continuous distribution of pore sizes from r_{min} to r_{max}. The number of pores within an arbitrary plane of cross-sectional area A and with radius between r_p and $r_p + dr_p$ is denoted by $\bar{g}(r_p)A\,dr_p$. The pore distribution function $\bar{g}(r_p)$ is given by

$$\bar{g}(r_p) = \theta/2\pi\beta r_p^3 \qquad (5)$$

where $\bar{g}(r_p)$ indicates an average over all inclination angles between the axis of the pore and the normal to the plane. Due to the random orientation of the pores, the intersection of a circular cylinder with a plane is an ellipse of average area $2\pi r_p^2$. Hence, the porosity is the $2\pi r_p^2$ moment of $\bar{g}(r_p)$ and the internal surface area is the $4\pi r_p$ moment of $\bar{g}(r_p)$.

The above expression for $\bar{g}(r_p)$ was derived from statistical arguments and was subsequently validated for coal char through comparison of the predicted volume and surface area distributions with mercury intrusion data (Simons and Finson, 1979). Mercury intrusion data generally demonstrate a linear increase in the intrusion volume with $\ln(r_p)$. It is the functional form of this relationship,

$$Pore\ Volume \propto \int_{r_{min}}^{r_p} r_p^2\ \bar{g}(r_p)\,dr_p \propto \ln r_p \qquad (6)$$

that depicts the inverse cubic dependence of $\bar{g}(r_p)$ on r_p. Mercury intrusion data has been used to validate this pore size distribution function for coal and char derived from that coal (Kothandaraman et.al., 1984), sorbents (Simons and Garman, 1986), catalysts, and even kidney stones from both men and women. There is, however, no such validation for soil or sediments available.

The number of pores within the bulk volume V whose pore radius is between r_p and $r_p + dr_p$ may be defined by $V f(r_p)\,dr_p$. The pore volume is expressed as the $\pi r_p^2 l_p$ moment of $f(r_p)$ and the internal surface area is the $2\pi r_p l_p$ moment of $f(r_p)$. The pore size distribution functions ($f(r_p)$ and $\bar{g}(r_p)$) are clearly not independent. The definitions of porosity and internal surface area infer that $f(r_p)$ is related to $\bar{g}(r_p)$ by

$$\bar{g}(r_p) = f(r_p)\,l_p/2 \qquad (7)$$

Equation (7) simply states that the probable number of pores intersecting an arbitrary plane increases with the length of the pore and with the density of pores.

The length of a pore is determined by an arbitrary intersection with another pore and is expressed (Simons and Finson, 1979) as a collision integral over the pore distribution functions. The analysis suggests that l_p , $\bar{g}(r_p)$ and $f(r_p)$ are proportional to r_p , $1/r_p^3$ and $1/r_p^4$ respectively. The constants of proportionality are obtained from integral constraints, i.e., the total porosity and internal surface area contained in the pore structure. The expression for $f(r_p)$ is given by

$$f(r_p) = \frac{\theta^{4/3}}{\pi\,\beta\,K_o\,r_p^4} \qquad (8)$$

where the constants were defined above.

The pore volume distribution corresponding to these distribution functions is similar to that utilized in the random pore model (Gavalas, 1980 & 1981). However, the pore tree model and the random pore model differ dramatically in their choice of the pore aspect ratio (length to diameter) and its implications with respect to pore branching. The random pore model allows a single pore to connect two larger pores. This picture lends itself to the idealization of instantaneous mixing between the pores and requires that the pore aspect ratio be of the order of one hundred. The pore tree theory uses data for r_{max} to imply (via K_o) that

8

all pores possess an aspect ratio of the order of ten. Hence, small pores may connect to larger pores only on one end and all pores must branch from successively larger pores like a tree or river system.

Each pore that reaches the exterior surface of the particle is depicted as the trunk of a tree. The size distribution of tree trunks on the exterior surface of the particle is denoted by $\bar{g}(r_t) 4\pi a^2 dr_t$ where $\bar{g}(r_t)$ is functionally identical to $\bar{g}(r_p)$. Each trunk of radius r_t is associated with a specific tree-like structure. Let N_t be defined as the branch distribution function where $N_t dr_p$ is the number of pores of radius r_p (within size range dr_p) in a tree whose trunk radius is r_t. The total number of pores of radius r_p in a sphere of radius a may be expressed as $4/3 \pi a^3 f(r_p) dr_p$ or, as the sum of all pores of radius r_p contained within every tree in the porous sample, plus all pores of radius r_p that are themselves the trunk of a tree. Hence,

$$\frac{4}{3}\pi a^3 f(r_p) = \int_{r_p}^{r_{max}} N_t \bar{g}(r_t) 4\pi a^2 dr_t + 4\pi a^2 \bar{g}(r_p) \tag{9}$$

where only trees with trunk radius greater than r_p will contain a pore of radius r_p. Using the previously derived expressions for r_{max}, $\bar{g}(r_p)$ and $f(r_p)$, Eq.(9) is identically satisfied by

$$N_t = r_t^3 / r_p^4 \tag{10}$$

The branch distribution function completely characterizes the pore tree. The internal surface area and pore volume associated with each pore tree are denoted by $S_t(r_t)$ and $V_t(r_t)$, respectively, and are expressed as the sum of the contributions from the trunk and that from the branches.

$$S_t(r_t) = 2\pi r_t l_t + \int_{r_{min}}^{r_t} 2\pi r_p l_p N_t dr_p \tag{11}$$

$$V_t(r_t) = \pi r_t^2 l_t + \int_{r_{min}}^{r_t} \pi r_p^2 l_p N_t dr_p \tag{12}$$

Using Eq.(10) for N_t, $S_t(r_t)$ and $V_t(r_t)$ become

9

$$S_t(r_t) = 2\pi r_t l_t \left(\frac{r_t}{r_{min}}\right)(1-\theta) \tag{13}$$

$$V_t(r_t) = \pi r_t^2 l_t \left(1+\ln\left(\frac{r_t}{r_{min}}\right)\right) \tag{14}$$

where the $(1-\theta)$ term in S_t has been included to account for pore combination (Simons, 1979a).

The surface area associated with the pore tree may be several orders of magnitude greater than the surface area of the trunk. However, the volume of the pore tree may, at most, be one order of magnitude greater than that of the trunk. It should also be noted that the above expressions for S_t and V_t reduce to those appropriate to a single cylindrical pore in the limit of $r_t \rightarrow r_{min}$ (the leaf of the tree). Furthermore, the integrals of $S_t(r_t)$ and $V_t(r_t)$ over all $\bar{g}(r_t)$ recover the total internal surface area and pore volume of the porous sample.

Each trunk of radius r_t is associated with a specific tree-like structure with continuous branching to ever decreasing pore radii. The radius and number of pores is a unique function of the distance x into the tree. The coordinate x is skewed in that it follows a tortuous path through the branches of the tree. Let n(x) represent the number of pores of radius r_p at location x in a tree of trunk radius r_t. An analysis (Simons,1982) of this pore tree has demonstrated that

$$n(x) = r_t^2 / r_p^2(x) \tag{15}$$

and the coordinate x is related to r_p by

$$dr_p/dx = -r_p/l_t \tag{16}$$

The continuous branching model has been used to successfully describe char oxidation (Simons, 1979b; Lewis and Simons, 1979; Simons, 1982 & 1983a), coal pyrolysis (Simons, 1983b & 1984) and the catalytic cracking of benzene by porous iron oxides (Simons et al., 1986). It was also used to successfully describe sulfur sorption (SO_2 and H_2S) by porous calcine (CaO) in the limit of zero utilization (Simons and Rawlins, 1980; Simons et al., 1984) and was later extended to include $CaSO_4$ and CaS deposits (Simons and Garman, 1986; Simons et al., 1987; Simons, 1988). The subsequent determination of the controlling physical parameters led to a new concept for the optimization of the sulfur sorption process (Simons, 1991; Simons et al., 1992) through spray drying of water soluble organic calcium solutions to control the sorbent pore structure.

III. INTERCONNECTIVITY

The first step in determining the size distribution of the interconnected pores and the distribution of the permeability is to determine the distribution function $\bar{G}_t(r_t,r_p)dr_p$ which represents the number of pores of radius r_p (within size range dr_p) per unit cross section of an arbitrary plane and also contained within a tree whose trunk radius is r_t. Consider an infinite homogeneous isotropic porous medium and isolate a spherical volume of that medium denoted by the radius a. Such a volume is illustrated in Fig. 10. The total number of pores of radius r_p (within size range dr_p) intersecting plane AA of area πa^2 has previously been defined by $\bar{g}(r_p)\pi a^2 dr_p$. The pores in plane AA in this size range may also be determined by integrating $\bar{G}_t(r_t,r_p)\pi a^2 dr_p$ over all trees whose trunk intersects the exterior surface of the porous sample. Hence it follows that

$$\bar{g}(r_p)\pi a^2 dr_p = \int_{r_p}^{r_{max}} [\bar{G}_t(r_t,r_p)\pi a^2 dr_p]\, \bar{g}(r_t)\, 4\pi a^2 dr_t \qquad (17)$$

where only those trees whose trunk radius is greater than r_p may contain a pore of radius r_p.

A solution to Eq. (17) for $\bar{G}_t(r_t,r_p)$ will not necessarily be unique. Physical arguments will help determine $\bar{G}_t(r_t,r_p)$ and help ensure that it is the particular solution we seek. Since N_t represents the number of pores of size r_p in the tree and the probability of a pore intersecting a plane is proportional to its length, it follows that $\bar{G}_t(r_t,r_p)$ should be
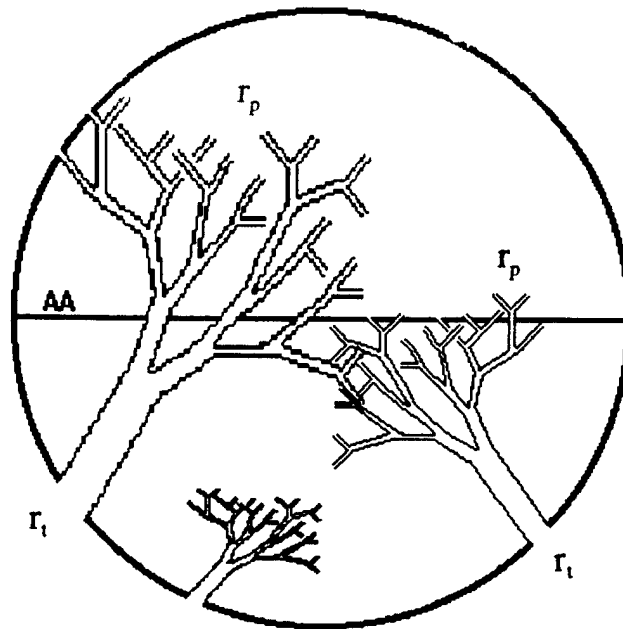

Figure 10. Spherical Volume of a Porous Medium

11

proportional to the product of N_t and l_p/l_t, i.e., proportional to r_t^2/r_p^3. Eq. (17) is identically satisfied by a function which differs from r_t^2/r_p^3 by $\ln(r_p)$.

$$\bar{G}_t(r_t, r_p) = \frac{r_t^2}{4\pi a^2 r_p^3 \ln(r_{max}/r_p)} \tag{18}$$

Note that $\ln(r_p/r_{max})$ introduces an integrable singularity at $r_p = r_{max}$ such that $\bar{G}_t(r_t, r_p)\,dr_p$ is finite at $r_p = r_{max}$. Hence, there is one and only one largest pore for each reference sphere.

The probability of trees sharing common branches, i.e., the interconnectivity of the pore structure is described in Fig. 11. We seek the distribution function $\bar{I}(r_p)\,dr_p$ which represents the number of pores (within size range dr_p about r_p) per unit area of plane AA that are connected to both sides of the pore structure through pores at least as large as r_p. A_θ is defined as the area within plane AA that is **open to one side** of the porous medium through all trees of size r_t' (through all pores of size r_p' that are at least as large as r_p). Subsequently, $A_\theta\,\bar{G}_t(r_t, r_p)\,dr_p$ represents the number of pores of size r_p (within size range dr_p) per unit area of plane AA that are contained in a tree of size range dr_t about r_t **and are also connected to the opposite side of the porous medium** through all trees denoted by r_t'. It follows that the distribution function for interconnected pores in plane AA may be obtained by integrating $A_\theta\,\bar{G}_t(r_t, r_p)\,dr_p$ over all trees (r_t) that are large enough to contain a pore of size r_p. Hence,

$$\bar{I}(r_p)\pi a^2\,dr_p = \int_{r_p}^{r_{max}} [A_\theta\,\bar{G}_t(r_t, r_p)\,dr_p]\,\bar{g}(r_t)2\pi a^2\,dr_t \tag{19}$$
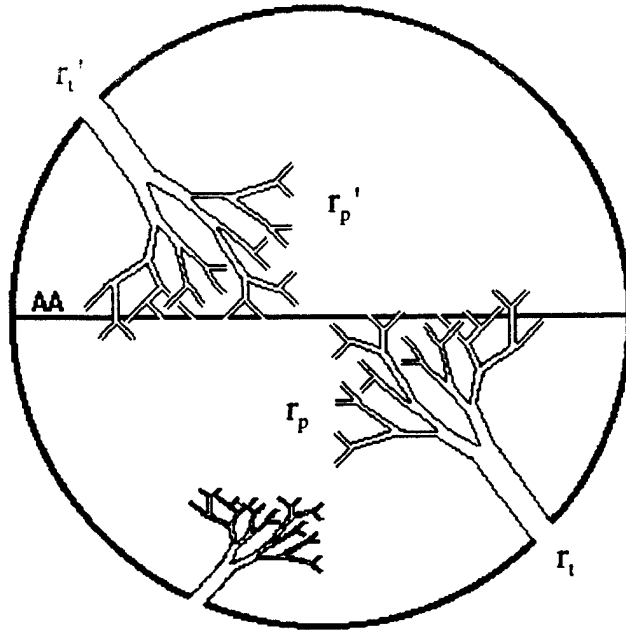

Figure 11. Interconnectivity of a Porous Medium

12

From the above definition of A_θ, A_θ may be expressed as

$$A_\theta = \int_{r_p}^{r_{max}} [\int_{r_p}^{r_t} 2\pi r_p^2 \, \pi a^2 \bar{G}_t(r_t, r_p) \, dr_p] \, \bar{g}(r_t) \, 2\pi a^2 \, dr_t \tag{20}$$

where the primes on the variables of integration have been omitted. Evaluating Eq. (20) yields

$$A_\theta = \frac{\pi a^2 \theta \ln(r_{max}/r_p)}{2\beta} \tag{21}$$

from which Eq. (19) yields the common branch distribution function.

$$\bar{I}(r_p) = \frac{\theta \ln(r_{max}/r_p)}{4\beta} \, \bar{g}(r_p) \tag{22}$$

It has been deduced that the total number of common branches of size r_p in an arbitrary plane scales approximately with the total number of pores of that size in that plane. Hence, there is a probability of interconnectivity at pore size r_p that is logarithmic in pore size. Defining this probability as $P_I(r_p)$ via Eq. (22),

$$P_I(r_p) = \frac{\theta \ln(r_{max}/r_p)}{4\beta} \tag{23}$$

it is apparent that approximately one percent of all pores of all sizes are interconnected through larger pores.

The broad size range associated with the interconnectivity suggests that a very wide range of pore sizes control transport and that a complicated mixture of convective and diffusive transport persists through all of pore space. While permeability is dominated by the largest pores, it is important to determine the level of convection that is occurring in smaller pores in order to accurately describe the fine scale transport necessary to assess chemical reactions. The ability of this pore structure model to describe bulk permeability, bulk diffusivity and the small scale convection responsible for hydrodynamic dispersion (Garabedian et al., 1991) are demonstrated before attempting to couple the chemical reactions to the macroscopic transport.

IV. PERMEABILITY

Poiseuille's law for laminar flow through a cylindrical pore relates the volume flow rate $\dot{Q}_p$ to the pore radius r_p, the viscosity of the fluid μ, and the pressure gradient $\dfrac{dP}{dx}$

$$\dot{Q}_p = \frac{\pi r_p^4}{8\mu}\left(-\frac{dP}{dx}\right) \tag{24}$$

whereas the average volume flow rate $\dot{Q}$ across the cross sectional area A of a porous medium is used to define the bulk permeability (k) by Darcy's law

$$k = \frac{\dot{Q}\mu}{A(-dp/dx)} \tag{25}$$

To determine the permeability, the pore volume flow rate must be related to the average volume flow rate. Convection across plane AA in Fig. 2 will possess contributions from two primary sources illustrated in Figs. 2a and 2b. Fig. 2a illustrates the case where the convection in plane AA is due solely to the pores that are interconnected in that plane. Fig. 2b illustrates the case where the convection in plane AA is due to the smaller pores in the pore tree that are interconnected outside of plane AA. This connectivity will translate into a slower velocity in the pore crossing plane AA but could be significant because 99% of the pores in plane AA are not interconnected in that plane.

Consider any pore of radius r_s in plane AA of Fig. 2b to be the trunk of a tree. Each pore of size r_p within the tree possesses the probability $P_I(r_p)$ of being interconnected and each interconnected pore in the tree will carry volume flow rate $\dot{Q}_p(r_p)$. Since there are $N_s dr_p$ (Eq. 10: $N_s = r_s^3/r_p^4$) pores in size range dr_p within the tree, the total volume flow rate $\dot{Q}_\infty(r_s)$ through trunk r_s in plane AA becomes

$$\dot{Q}_\infty(r_s) = \int_{r_{min}}^{r_s} \dot{Q}_p(r_p)\, P_I(r_p)\, N_s\, dr_p \tag{26}$$

or, for $r_{max} >> r_s$,

$$\dot{Q}_\infty(r_s) = \frac{\theta\pi r_s^4 \ln(r_{max}/r_s)}{32\mu\beta}\left(-\frac{dp}{dx}\right) + \textit{Higher Order Terms} \tag{27}$$

14

Within this approximation, it is seen that $\dot{Q}_\infty(r_s)$ is identical to the volume flowing through the pores that are interconnected within plane AA. i.e.,

$$\dot{Q}_\infty(r_s) \equiv \dot{Q}_p(r_s) \; P_I(r_s) \tag{28}$$

which demonstrates that all volume flow through plane AA in pore size r_s is dominated by the interconnectivity of size r_s in plane AA and not by the interconnectivity of smaller pores in subsequent branches of the pore tree. Simply stated: case 2a dominates case 2b.

Since all volume flow through plane AA is limited by the interconnectivity of the pores in that plane, the total volume flow rate $\dot{Q}$ is obtained by integrating Eq. (24) over all interconnected pores in area A. Hence,

$$\dot{Q} = \frac{\pi A}{8 \, \mu} \left(-\frac{dP}{dx} \right) \int_{r_{min}}^{r_{max}} r_p^4 \; \overline{I}(r_p) \, dr_p \tag{29}$$

where $\overline{I}(r_p)$ is the "common branch distribution function" given by Eq. (22). The bulk permeability (k) is then expressed as

$$k = \frac{\pi}{8} \int_{r_{min}}^{r_{max}} r_p^4 \; \overline{I}(r_p) \, dr_p \tag{30}$$

Upon integration, Eq. (30) becomes

$$k = \left(\frac{\theta \, r_{max}}{16 \, \beta} \right)^2 \tag{31}$$

Equation (31) resembles a dozen other expressions (Dullien, 1979) for permeability wherein it is concurred that the bulk permeability is dominated by the largest pores in the medium but the unknown value of that permeability is simply replaced by an unknown fiber or pore size to the second power. Since the pore size distribution function will be least accurate at the extreme end of the size range, i.e. at r_{max} , no claim can possibly be made that the numerical constants in Eq. (31) are in any way superior to those derived elsewhere. One important advantage of the extended pore tree model is that it characterizes the distribution of permeability in pore space, a feature that will be important in describing fine scale contaminant transport and in-situ remediation. A second advantage is the ability to assess statistical errors in the measurement of the permeability as a function of the measurement scale size. This exercise is also a good test of the extended pore tree model.

Consider a soil sample with the following physical characteristics:

Conductivity:	$v = 2$ cm/hr
Permeability:	$k = 0.6$ Darcy
Porosity:	$\theta = 50\%$
Pore Aspect Ratio:	$K_o = 5$
$\ln(r_{max}/r_{min})$	$\beta = 12$

From Eq. (31), it follows that

$$r_{max} = 300 \ \mu m$$

and subsequently $r_{min} = 20$ Å. The size of the smallest pore is not an important parameter for this application but may be readily adjusted through a minor variation in the value of β (e.g., for r_{min} of the order of 100 Å, $\beta = 10$). The bold assertion made in applying this pore structure model to soil is that the $1/r_p^3$ pore size distribution is valid between r_{min} and r_{max}.

To investigate the role of the measurement scale size on permeability, consider the largest pore r_{max} contained in the spherical sample of radius "a" as given by Eq. (1). Since r_{max} in Eq. (31) for the permeability represents the largest pore in the medium, the corresponding value of "a" is denoted a_{max} and represents the largest sample size for which the pore sizes will scale with the dimensions of the sample. From Eqs. (1) and (31)

$$a_{max} = \frac{24 K_o \beta}{\theta^{4/3}} \sqrt{k} \tag{32}$$

Each sphere of radius a_{max} will contain <u>one</u> pore of size r_{max}. A 20 x 20 grid of these spheres will be characterized by the dimension $40a_{max}$ and contain 400 pores of size r_{max}. Each of these pores possess probability $P_I(r_p)$ of being interconnected. Following Eq. (23), $P_I(r_p)$ is approximately 0.0025 for r_p sufficiently close to r_{max}. Hence, only <u>one</u> of the 400 largest pores in this 20 x 20 grid will be interconnected and the error in the measurement of the permeability will correspond to the statistical error of 100% associated with that of a sample number of unity. Carrying this argument to a 200 x 200 grid of dimension $400a_{max}$, there will be 100 interconnected pores corresponding to a statistical error of 10%. Similarly, a grid of scale $4000a_{max}$ will reduce the error to 1%.

Figure 3 illustrates the predicted permeability measurement error associated with the soil sample characterized above ($a_{max} = 0.3$ cm). Note that the errors associated with the measurement of permeability become negligible as the measurement scale size approaches several meters. This has been confirmed by the infiltration data of Shouse et. al. (1994). The measured value of hydraulic conductivity asymptotes to 2 cm/hr at measurement scales greater than 4 meters. At smaller measurement scales, the inferred measurement error is calculated under the assumption that the asymptote is precisely 2 cm/hr. The excellent agreement between the predicted and inferred error supports the extension of the pore tree model to describe porous permeable media.

V. BULK GASEOUS DIFFUSION IN PARTIALLY SATURATED MEDIA

The extended pore tree model is readily adapted to partially saturated media through the assumption that all of the water is contained in pore sizes between r_{min} and r_{sat} while only gas is contained between r_{sat} and r_{max}. Since, by Eq. (6), porosity is distributed as $\ln(r_p)$ in pore space, the porosity associated with the air filled pores (θ_a) is approximated by

$$\theta_a = \frac{\ln(r_{max}/r_{sat})}{\beta} \theta \qquad (33)$$

where r_{sat} is treated as an independent variable of the saturated pore structure. No gaseous diffusion is allowed within $r_p \leq r_{sat}$. It is demonstrated that the gas diffusivity scales as $1/r_{sat}$ and it is the sensitivity of r_{sat} to the saturated volume that controls the saturated diffusivity.

The diffusive mass flux in a single pore is given by

$$\dot{M}_p(r_p) = \pi \, D_g \, r_p^2 \left(\frac{-\partial \rho_c}{\partial x} \right) \qquad (34)$$

where D_g is the continuum gas diffusion coefficient ($D_g = 0.2$ cm^2/s). Just as in the case of convection, it must be determined whether the mass flux across plane AA in Fig. 2 is determined by the interconnectivity of the smaller pores out of the plane (Fig. 2b) or by only those pores that are interconnected in the plane (Fig. 2a). Consider any pore of radius r_s in plane AA of Fig. 2b to be the trunk of a tree. Each pore of size r_p within the tree possesses the probability $P_I(r_p)$ of being interconnected and each interconnected pore in the tree will carry the mass flow rate $\dot{M}_p(r_p)$. Since there are $N_s dr_p$ (Eq. 10: $N_s = r_s^3/r_p^4$) pores in size range dr_p within the tree, the total mass flow rate $\dot{M}_\infty(r_s)$ through each and every trunk of radius r_s in plane AA becomes

$$\dot{M}_\infty(r_s) = \int_{r_{sat}}^{r_s} \dot{M}_p(r_p) \; P_I(r_p) \; N_s \; dr_p \qquad (35)$$

Integration of Eq. (35) yields the mass flux (case 2b) for each trunk of radius r_s

$$\dot{M}_\infty(r_s) = \frac{\pi \, D_g \, \theta_a \, r_s^3}{4 r_{sat}} \left(\frac{-\partial \rho_c}{\partial x} \right) \qquad (36)$$

where a $\ln(r_{max}/r_{sat})$ term was eliminated via Eq. (33) and it has been assumed that $r_s >> r_{sat}$. This introduces an error for the smaller trees close to r_{sat} but since bulk diffusion (D_{bulk}) will

17

be shown to be dominated by the largest trees, the approximation is valid.

If the mass flux through plane AA is limited by the pores that are interconnected in that plane (case 2a), the mass flux is expressed as $\dot{M}_p(r_s) P_I(r_s)$, and it is immediately seen that

$$\dot{M}_\infty(r_s) > \dot{M}_p(r_s) P_I(r_s) \tag{37}$$

i.e., case 2b dominates case 2a. Since the mass diffusion in plane AA is determined by the pore interconnectivity of the smaller pores outside of plane AA, the saturation of those smaller pores becomes an important element in the bulk gaseous diffusion.

Since each pore of radius r_s in plane AA carries mass flux $\dot{M}_\infty(r_s)$, the bulk diffusion coefficient is obtained by integrating Eq. (36) over all pores in that plane

$$D_{bulk} = \int_{r_{sat}}^{r_{max}} \frac{\pi D_g \theta_a r_s^3}{4 r_{sat}} \bar{g}(r_s) dr_s \tag{38}$$

subject to the approximation that the gas is contained in the largest pores ($r_{max} >> r_{sat}$).

$$D_{bulk} = \frac{D_g \theta \theta_a r_{max}}{8 \beta r_{sat}} \tag{39}$$

Eliminating r_{max} via Eq. (31), the bulk diffusivity D_{bulk} is expressed in terms of the permeability k.

$$D_{bulk} = \frac{2 D_g \theta_a \sqrt{k}}{r_{sat}} \tag{40}$$

The bulk diffusivity cannot increase indefinitely with increasing permeability as inferred by Eq. (40). In deriving this expression, the mass flux through the interconnected branches of the tree was not constrained from exceeding the diffusive capabilities of the trunk itself. To correct this potential problem, the limit of D_{bulk} is determined as the maximum diffusive flux (i.e., D_g) in pore r_s integrated over all pores in plane AA.

$$D_{limit} = \int_{r_{min}}^{r_{max}} \pi D_g r_s^2 \bar{g}(r_s) dr_s = \frac{D_g \theta}{2} \tag{41}$$

18

D_{limit} is indicative of existing models for the diffusivity within a completely connected pore structure and is illustrated in Figure 4 together with the predicted values of D_{bulk} for an extended range of values of permeability and the saturation radius, r_{sat}.

Model predictions correspond to the measured values of $\theta_a = 0.2$ and $\theta = 0.5$ from Washington et. al., (1994), and the diffusivity data suggest a value of r_{sat} in the range of 10 µm to 100 µm. An exact comparison of the present theory to the least squared fit obtained by Washington et. al., (1994), suggests a value of 30 µm. This least squared fit also demonstrates a permeability dependence of the power 0.53 whereas the model predicts 0.5.

While the excellent agreement of the model with the data of Washington et. al., (1994) does substantiate the present theory, it is apparent that there is a very wide range of possible values for D_{bulk} in partially saturated soils which will depend upon an unknown saturation radius. A two order of magnitude decrease in the saturation radius will increase the bulk diffusivity by two orders of magnitude and yet the corresponding increase in the air filled porosity is, by Eq. (33), only 33%. Hence, field measurements of the unsaturated volume are not sufficiently accurate to correlate bulk diffusivities. If bulk diffusivities are to be correlated with field data, such measurements should attempt to measure the saturation radius.

19

VI. HYDRODYNAMIC DISPERSION

The distribution of velocity (or volume flux) with pore size has been utilized to develop a description of hydrodynamic dispersion (Simons, 1996b). The volume flux $\dot{Q}_p$ through a single pore of radius r_p subjected to a pressure gradient $\dfrac{dp}{dx}$ is given by Eq. (24).

$$\dot{Q}_p(r_p) = \frac{\pi r_p^4}{8\mu}\left(-\frac{dp}{dx}\right) \tag{42}$$

The corresponding fluid velocity $v_p(r_p)$ within that single pore is

$$v_p(r_p) = \frac{r_p^2}{8\mu}\left(-\frac{dp}{dx}\right) \tag{43}$$

and it is evident that the fluid within the larger pores will convect ahead of the fluid in the smaller pores inducing an apparent diffusional process commonly referred to as hydrodynamic dispersion.

It has been shown (Eq. 28) that the volume flux $\dot{Q}_\infty(r_p)$ within all pores of radius r_p across a fixed plane is limited by the interconnectivity $P_f(r_p)$ of the pore structure

$$\dot{Q}_\infty(r_p) = \dot{Q}_p(r_p)\, P_f(r_p) \tag{44}$$

and the total volume flow rate $\dot{Q}$ across the cross sectional area A of the pore structure is obtained by integrating Eq. (44) over all pores in that cross section. Using the pore size distribution function denoted by $\bar{g}(r_p)$, $\dot{Q}$ becomes

$$\dot{Q} = \int_{r_{min}}^{r_{max}} \dot{Q}_\infty(r_p)\, \bar{g}(r_p) A\, dr_p \tag{45}$$

from which permeability k is defined as

$$k = \frac{\dot{Q}\mu}{A\,(-dp/dx)} = \left(\frac{\theta\, r_{max}}{16\beta}\right)^2 \tag{46}$$

and the mean pore velocity $\bar{v}$ is defined as the average fluid velocity over the porous area.

$$\bar{v} = \frac{\dot{Q}}{\theta A} = \frac{k(-dp/dx)}{\theta \mu} \tag{47}$$

The mean velocity associated with the pore radius r_p is denoted by $v_m(r_p)$ and it is the variation of $v_m(r_p)$ about $\bar{v}$ that causes the "diffusion" or hydrodynamic dispersion of a specific species about the mean convection velocity $\bar{v}$. The aggregate fluid velocity from plane to plane must be determined as a function of pore radius. In any given cross sectional plane, the fraction $P_f(r_p)$ of the pores were determined to be interconnected and carry fluid velocity $v_p(r_p)$ while the non-interconnected pores in that size range do not support a significant fluid velocity. This was interpreted as an effective fluid velocity $v_p(r_p) P_f(r_p)$ occurring in all pores of radius r_p in a given cross sectional plane. An expression for $v_m(r_p)$ is utilized which scales with $v_p(r_p) P_f(r_p)$ and recovers the mean convection velocity $\bar{v}$ in the limit of $r_p = \bar{r}_p$, where $\bar{r}_p$ is the pore size associated with velocity $\bar{v}$ and is yet to be determined.

$$\frac{v_m(r_p)}{\bar{v}} = \frac{r_p^2 \ln(r_{max}/r_p)}{\bar{r}_p^2 \ln(r_{max}/\bar{r}_p)} \tag{48}$$

The mean velocity associated with pores of size r_p will be used to relate a species concentration profile in pore space to that in physical space using

$$\frac{v_m(r_p)}{\bar{v}} = \frac{x}{\bar{v} t} \tag{49}$$

where x is a spatial coordinate in the concentration profile. That profile will contain the concentration $\bar{c}$ moving with mean velocity $\bar{v}$ and associated with pore size $\bar{r}_p$ were both $\bar{c}$ and $\bar{r}_p$ are yet to be determined. The system will lead to the "diffusion" or hydrodynamic dispersion of a specific species about the concentration $\bar{c}$ moving with the mean convection velocity $\bar{v}$.

From Eq. (48) it is seen that the mean velocity associated with pores of size r_p possesses a relative maximum at $r_{max}/\sqrt{e}$ as illustrated in Figure 5. Let r_1 and r_2 represent the two values of r_p corresponding to a particular value of $v_m(r_p)$. Clearly, the fluid in the pore of radius $r_{max}/\sqrt{e}$ convects ahead of that in the pores of radius r_1 and r_2. Consider flow

21

in a saturated porous medium in which all fluid behind a fixed plane normal to the flow is suddenly injected with red dye. All dyed fluid in pores whose radius is between r_1^* and r_2^* will translate with velocity equal to or greater than v_m^* and move to a corresponding location x^* or greater. The concentration profile $c(x)/c_o$ of the red dye at location x will scale with the volume flux whose velocity is greater than $v_m(x)$ from within pores whose radius is between $r_1(v_m(x))$ and $r_2(v_m(x))$. From these arguments, it follows that the normalized concentration profile is given by

$$c(x)/c_o = \int_{r_1}^{r_2} \dot{Q}_\infty(r_p)\,\bar{g}(r_p)\,dr_p \, / \int_{r_{min}}^{r_{max}} \dot{Q}_\infty(r_p)\,\bar{g}(r_p)\,dr_p \qquad (50)$$

where $r_1(v_m(x))$ and $r_2(v_m(x))$ are related through Eq. (48),

$$r_1^2 \ln(r_{max}/r_1) = r_2^2 \ln(r_{max}/r_2) \qquad (51)$$

and $c(x)/c_o$ becomes

$$c(x)/c_o = (r_2^2 - r_1^2)/r_{max}^2 \qquad (52)$$

The concentration profile of the red dye in pore space is readily obtained by solving Eq. (51) for r_1/r_{max} and r_2/r_{max} parametric in terms of r_1/r_2 between zero and unity. The corresponding dye concentration profile in pore space is illustrated in Figure 12. Note that the pore containing the largest velocity corresponds to the "front" of the spatial profile (Figure 6) where c=0 and the pores containing the lower velocities are at the rear of the spatial profile where c tends to unity.
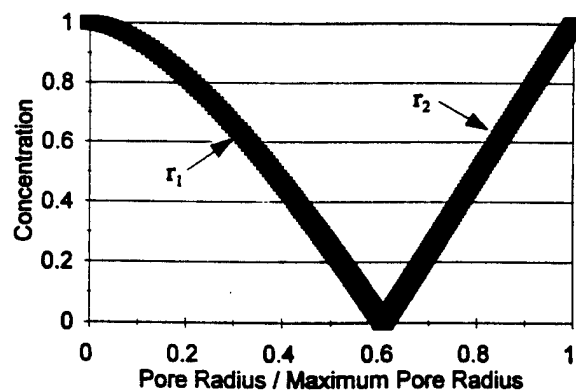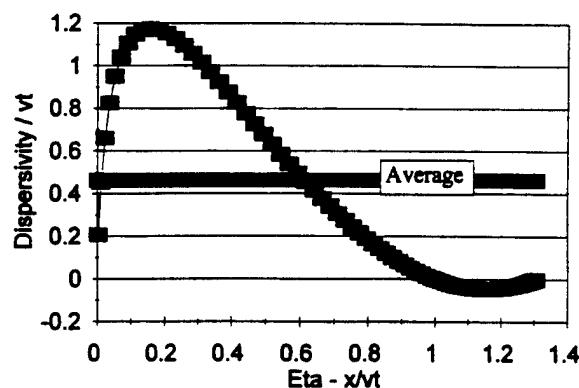

Figure 12. Concentration in Pore Space   Figure 13. Hydrodynamic Dispersivity

22

Eq. (50) represents the concentration profile of the red dye in pore size space, pore velocity space, and physical space. The concentration $\bar{c}$ associated with the mean velocity $\bar{v}$ may be determined from the conservation of the flux of the concentration profile. This is expressed as

$$\left(\frac{\bar{c}}{c_o}\right) \bar{v}\,\theta\,A = \int_{r_{min}}^{r_{max}} \left(\frac{c(r_p)}{c_o}\right) \dot{Q}_\infty(r_p)\,\bar{g}(r_p)\,A\,dr_p \tag{53}$$

where the integral is split into integrals over the r_1 and r_2 branches and obtained numerically from the profile illustrated in Figure 12. Integration yields

$$\bar{c}/c_o = 0.5 \tag{54}$$

It is seen from Figure 12 that there are two pore radii in pore space that satisfy Eq. (54). On the r_1 branch $\bar{r}_p$ is 0.38332 r_{max} and on the r_2 branch we obtain 0.80428 r_{max}. In each case

$$(\bar{r}_p^2 / r_{max}^2)\,\ln(r_{max}/\bar{r}_p) = 0.1409 \tag{55}$$

and Eqs. (48) and (49) assign a unique value of x to each value of r_1 and r_2. We define

$$\eta = \frac{x}{\bar{v}t} = \frac{r_1^2}{r_{max}^2}\frac{\ln(r_{max}/r_1)}{0.1409} \tag{56}$$

and/or the identical expression in r_2. The concentration profile may be expressed in physical space as a function of η corresponding to that in pore space as a function of r_1 and r_2. The concentration profile in physical space is illustrated in Figure 6 where all red dye would be located at the location $\eta = 1$ were it not for the velocity variation within pore size. The "front" of the concentration profile has progressed 30% ahead of the mean while the slower fluid in the smaller pores has trailed considerable.

If we were standing at the end of a porous flow tube, the concentration passing our location would exhibit a time dependence (c vs. $1/\eta$) illustrated in Figure 7. The faster fluid breaks through ahead of the mean flow ($\bar{c}/c_o = 0.5$) while the fluid in the smaller pores is delayed. Data of Elrich, et al., (1966), as reported by Brusseau and Rao (1989), are illustrated in Fig. 8 and support the current theory of hydrodynamic dispersion. While the long "tail" of the concentration profile is generally attributed to nonequilibrium, the current pore structure model attributes it to the wide pore size distribution occurring in soil. The narrow pore size distributions occurring in laboratory "soil" will yield a much narrower concentration profile, i.e., less hydrodynamic dispersion.

The local value of the dispersivity required for the concentration profile to be compatible with the diffusion equation reflects the virtue of expressing hydrodynamic dispersion as a Fickian process. The hydrodynamic dispersion (D_h in length^2/time) normalized by the mean velocity $\bar{v}$ is the dispersivity λ. The dispersivity normalized by the mean convection distance $\bar{v}t$ is expressed in terms of the concentration profile via

$$\frac{\lambda}{\bar{v}t} = \frac{(1-\eta)\,\partial c/\partial \eta}{\partial^2 c/\partial \eta^2} \tag{57}$$

and illustrated in Figure 13. Figure 13 illustrates that neither λ nor $\lambda/\bar{v}t$ is constant, i.e., the concentration profile could never be described by a Fickian process. Future research will be directed toward using this analytic pore structure/ pore transport model to help derive an analytic expression for hydrodynamic dispersion that replaces the Fickian process in the transport equations.

VII. COUPLING SUBSCALE REACTIONS TO MACROSCOPIC TRANSPORT

Analysis of the permeability, bulk diffusivity, and hydrodynamic dispersion has utilized the interconnectivity of the pores to determine the distribution of the convection velocity with pore size. This analysis suggests the existence of a permeable sub-range in the pore structure which does not contribute significantly to the bulk permeability but in which convection dominates diffusion. It is the balance of the sub-scale convection with the small scale diffusion that will control contaminant transport and in-situ remediation. The size distribution of the pores and grains, and the variations in fluid velocity within and between pores of different sizes is critical to interfacing the transport processes. A methodology is developed to couple subscale diffusion, convection and chemical reactions to the macroscopic transport in order to accurately describe contaminant transport and in-situ remediation in Ground Water Simulation codes.

A typical species transport equation in permeable soil is of the form:

$$\frac{\partial c}{\partial t} + \bar{v} \frac{\partial c}{\partial x} = D_h \frac{\partial^2 c}{\partial x^2} + \frac{c\dot{M}}{M} \tag{58}$$

where c is the local species concentration, $\bar{v}$ is the mean convection velocity as determined by the local pressure gradient and permeability k, and D_h is the hydrodynamic dispersion. The $\partial c/\partial t$ term is the true unsteady term and the source and/or sink of species c due to chemical and/or physical processes within the subscale pore structure is written as $c\dot{M}/M$ where $\dot{M}/M$ represents a bulk rate (1/t) of production or consumption. The bulk rate $\dot{M}/M$ will be related to gradients of c on length scales of order millimeters within the subscale pore structure and cannot be expressed in terms of the $\partial c/\partial x$ of the macroscopic transport grid.

To describe the subscale chemical reactions and transport, a "grain" of soil of radius a_g is isolated from the rest of the medium. The grain size will be chosen sufficiently small that molecular diffusion and coupled chemical reactions will dominate the subscale transport. The pore tree was developed (Simons, 1982, 1983a, 1988) to treat coupled chemical reactions and molecular diffusion within immobile porous grains. A reactant species will diffuse into the pores and react on the walls of the pore. The chemical reaction on the walls of the pore establishes a species gradient which is greater than c/a_g and accelerates the molecular diffusion. The effective molecular diffusion coefficient is the square root of the product of the molecular diffusivity and the chemical rate constant. The solution for $\dot{M}$ in this limit scales as a_g^2 because transport is limited by diffusion across the surface area a_g^2 while the species gradient is independent of a_g. The particular form of the solution for contaminant transport and soil remediation will vary with the number of reactions and kinetic mechanisms but the fundamentals of the problem depict that $\dot{M}$ will scale as a_g^2 in this diffusive limit.

As the grain size is reduced, the diffusive abilities of the grain are able to keep up with the kinetics of the chemical reactions. The species concentration gradient becomes small

25

compared to c/a_g and the species reaction rate scales with the volume of the reactant. In this "kinetic limit," $\dot{M}$ will scale as a_g^3. Since the local mass of the reactant species M also scales as a_g^3, it follows that $\dot{M}/M$ scales as a_g^0 in the kinetic limit and as a_g^{-1} in the diffusive limit. This behavior is expressed as

$$\frac{\dot{M}}{M} = \dot{R}_1 \qquad (\textit{Kinetic Limit}: a_g < \dot{R}_2 / \dot{R}_1) \tag{59}$$

and

$$\frac{\dot{M}}{M} = \dot{R}_2 / a_g \qquad (\textit{Diffusive Limit}: a_g > \dot{R}_2 / \dot{R}_1) \tag{60}$$

where it is assumed that $\dot{R}_1$ and $\dot{R}_2$ may be rigorously determined for specific kinetic processes in soil through direct application of the pore tree/pore transport model.

The reactant species must be supplied to the edge of the grain at a rate compatible with the rate of species consumption within the grain. Convection in the subscale will transport the species across the cross section πa_g^2 at a rate depicted by the permeability k_g which is appropriate to the length scale a_g. Since $\dot{M}$ is $\rho \dot{Q} \pi a_g^2$ and $\dot{Q}$ may be obtained from equation (25), $\dot{M}/M$ becomes

$$\frac{\dot{M}}{M} = \frac{c\,\rho\,(k_g/\mu)(\pi a_g^2)(-dp/dx)}{c\,\rho\,\theta\,(4\pi a_g^3/3)} \tag{61}$$

where ρ is the density of the reactant species (gas or liquid phase). The integral for the permeability (Eq. 30) is dominated by the largest pores. If r_{mg} is the largest pore in the grain and r_{max} is the largest pore in the soil, k_g appropriate to the grain will scale with k, the permeability of the soil, via

$$\frac{k_g}{k} = \frac{(r_{mg})^2 (1 + 2\ln(r_{max}/r_{mg}))}{r_{max}^2} \tag{62}$$

where it is assumed that r_{max}/r_{mg} is roughly half the width of the entire pore distribution. i.e., the $(1+2\ln)$ term is approximately equal to β (Eq. 4).

The radius (r_{mg}) of largest pore in the grain of radius a_g is directly proportional to a_g just as r_{max} is directly proportional to a_{max}, the radius of the largest grain in which the pore size will scale with the dimension of the sample. Hence, equation (62) becomes

26

$$\frac{k_g}{k} = \frac{(a_g)^2 \beta}{a_{max}^2} \tag{63}$$

and, using Eq. (32) for a_{max}, Eq. (63) is rewritten as

$$\frac{k_g}{k} = \frac{a_g^2 \theta^{8/3}}{576 K_o^2 \beta k} \tag{64}$$

such that the convective limit of $\dot{M}/M$ follows.

$$\frac{\dot{M}}{M} = \frac{\theta^{5/3}(-dp/dx)}{768 \mu \beta K_o^2} a_g \equiv \dot{R}_3 a_g \quad (Convective \ Limit) \tag{65}$$

The convective limit of $\dot{M}/M$ does not explicitly depend on the bulk permeability k because k is controlled by the largest pores in the soil and cannot distribute the reactants on a scale as fine as these small grains.

These results are illustrated in Figure 9 and indicate that the convective limit increases with larger grains while the diffusive limit decreases with increasing grain size. The convective and diffusive limits are equal at $a_g = a_{eq}$

$$a_{eq} = (\dot{R}_2 / \dot{R}_3)^{1/2} \tag{66}$$

where it is apparent that for grains smaller than a_{eq}, the convection cannot keep up with the diffusion and for grains larger than a_{eq}, the diffusion cannot keep up with the convection. The system will attain a natural equilibrium at $a_g = a_{eq}$ and the corresponding value of $\dot{M}/M$ becomes

$$\frac{\dot{M}}{M} = Smaller \ Of \ [\ (\dot{R}_2 \dot{R}_3)^{1/2},\ \dot{R}_1\ ] \tag{67}$$

where it has been noted that the solution at $a_g = a_{eq}$ cannot exceed the limit of kinetic control.

The above expression for the bulk source and/or sink of species c due to chemical and/or physical processes within the subscale pore structure is incomplete without specific models for $\dot{R}_1$ and $\dot{R}_2$. Future research will be directed toward developing a library of such models. The most basic processes of contaminant diffusion and adsorption are briefly described below.

27

VIII. IMMOBILE SOLUTIONS: TWO LIMITING CASES

VIII.1 General Approach

The pore structure model described above has been coupled to a transport model (Simons, 1982) that is capable of describing the simultaneous action of diffusive and kinetically controlled processes in the immobile region. The pore transport model was developed to describe quasi-steady char oxidation in which both adsorption and desorption occur simultaneously. This transport model will be adapted to describe the transient chemisorption and remediation processes in soil such that we will be able to couple the subscale reactions to the macroscopic transport as described above.

Each pore that reaches the exterior surface of the particle is depicted as the trunk of a tree. The size distribution of tree trunks on the exterior surface of the particle is denoted by $\bar{g}(r_t)4\pi a^2 dr_t$ where $\bar{g}(r_t)$ is functionally identical to $\bar{g}(r_p)$. Each trunk of radius r_t is associated with a specific tree-like structure as illustrated in Fig. 1. A pore structure with continuous branching to ever decreasing pore radii is depicted as being attached to a uniform trunk of radius r_t. The radius and number of pores is a unique function of the distance x into the tree. The coordinate x is skewed in that it follows a tortuous path through the branches of the tree. Let n(x) represent the number of pores of radius r_p at location x in a tree of trunk radius r_t. An analysis (Simons,1982) of this pore tree has demonstrated that

$$n(x) = r_t^2 / r_p^2(x) \tag{68}$$

and the coordinate x is related to r_p and the length of the tree trunk l_t by

$$dr_p/dx = -r_p/l_t \tag{69}$$

When this porous structure is placed in an environment with a reactive gas, the reactive gas will diffuse into the pore tree and react with the material that constitutes the walls of the pore. The diffusion of the reactive gas through n pores of radius r_p is balanced by the continuous reaction of the gas at the walls of the pore. We write

$$\frac{d}{dx}\left(n \rho_g D_g \pi r_p^2 \frac{dc}{dx}\right) = n 2\pi r_p k_a p_g c \tag{70}$$

where c is the mass fraction of the reactant gas, D_g is the self diffusion coefficient of the reactant species, ρ_g is the combined density of all gases in the pore, p_g is the combined pressure (in atmospheres) of all gases in the pore, and k_a is the rate constant (g/s/cm^2/atm) for a continuous first order reaction which is a function of particle temperature alone.

28

The total reaction rate of the pore tree, $\dot{M}_t$, is related to the gradient of c at x=0 by

$$\dot{M}_t = -\rho_g D_g \pi r_t^2 \frac{dc}{dx}\Big|_o \qquad (71)$$

However, to obtain the value of dc/dx at x=0, Eq. (70) must be integrated subject to the boundary conditions that c=c$_o$ at x=0 (r_p =r$_t$) and dc/dx=0 at x=x$_t$ (r_p =r$_{min}$). The total reaction rate of the porous particle is obtained by integrating $\dot{M}_t$ over all trees

$$\dot{M}_T = \int_{r_{min}}^{r_{max}} \dot{M}_t 4\pi a^2 \bar{g}(r_t)\, dr_t \qquad (72)$$

The pore tree model has been used to successfully describe char oxidation (Simons, 1979b; Lewis and Simons, 1979; Simons, 1982 & 1983a), coal pyrolysis (Simons, 1983b & 1984) and the catalytic cracking of benzene by porous iron oxides (Simons et al., 1986). It was also used to successfully describe sulfur sorption (SO_2 and H_2S) by porous calcine (CaO) in the limit of zero utilization (Simons and Rawlins, 1980; Simons et al., 1984) and was later extended to include $CaSO_4$ and CaS deposits (Simons and Garman, 1986; Simons et al., 1987; Simons, 1988). The subsequent determination of the controlling physical parameters led to a new concept for the optimization of the sulfur sorption process (Simons, 1991; Simons et al., 1992) through spray drying of water soluble organic calcium solutions to control the sorbent pore structure. This transport model will be adapted to describe the transient chemisorption and remediation processes in soil such that we will be able to couple the subscale reactions to the macroscopic transport as described above.

VIII.2 Contaminant Adsorption in Saturated Media

Consider a contaminant in a completely saturated medium. The contaminant will diffuse into the pore structure (Figure 1) as described by Eq. (70). Assume that the diffusion is rate limiting and the kinetic term (adsorption rate) in Eq. (70) is relatively fast. Within this idealization, the walls of the pores between x=0 and x=x$_c$(t) will be completely contaminated while the walls of the pores for x>x$_c$(t) will not be contaminated. All of the reaction is assumed to occur at (at and around) x$_c$(t) where x$_c$(t) expands throughout the entire pore tree as time approaches infinity. The first integral of Eq. (70) between x=0 and x=x$_c$(t) becomes

$$n\rho_L D_L \pi r_p^2 \frac{dc}{dx} = -\dot{M}_t(x_c) \qquad (73)$$

where ρ_L denotes the liquid density, D_L denotes the contaminant diffusion coefficient and $\dot{M}_t(x_c)$ denotes the net mass flux of the contaminant into the pore tree as a function of time.

Using n(x) and dr_p/dx defined above, Eq. (73) may be integrated subject to the boundary condition that $c=c_o$ at $x=0$ $(r_p=r_t)$ and $c=0$ at $x=x_c$ $(r_p=r_c)$. The contaminant concentration in the liquid within the pore structure becomes

$$c = \frac{c_o \ln(r_p/r_c)}{\ln(r_t/r_c)}$$ (74)

and the net mass flux of the contaminant into the pore tree is given by

$$\dot{M}_t(x_c) = \frac{c_o \pi D_L \rho_L r_t^2}{l_t \beta}$$ (75)

where the $\ln(r_t/r_c)$ term has been replaced with β (Eq. 4).

The behavior of $\dot{M}_t(x_c)$ near complete contaminant adsorption (for r_c near r_{min}) is incorrect and an exact solution to Eq. (70) is required to precisely simulate this limit. However, Eq. (75) may be modified to more closely simulate the mass flux in the limit of complete contaminant adsorption. If the walls of the pore tree adsorb contaminant at the rate depicted by Eq. (75), the reaction will proceed until the entire surface area S_t of the pore tree is coated with contaminant. Denoting the maximum surface contaminant adsorption level as

σ_w (mass per unit area), the characteristic time τ over which Eq. (75) is valid is $\sigma_w S_t/\dot{M}_t$. Using Eq. (13) for the surface area S_t of the pore tree, τ becomes

$$\tau = \frac{2\sigma_w l_t^2 \beta}{c_o D_L \rho_L r_{min}}$$ (76)

and $\dot{M}_t(x_c)$ is rewritten as

$$\dot{M}_t(x_c) = \frac{c_o \pi D_L \rho_L r_t^2}{l_t \beta} \exp(-t/\tau)$$ (77)

The total adsorption rate of the porous grain is obtained by integrating $\dot{M}_t$ over all trees as in Eq. (72) above. At late time, the integral is dominated by the largest pore trees in the grain. The radius of the largest tree trunk is related to the grain size by equation (1) and the total adsorption rate of the porous grain is see to be

$$\dot{M}_T = \frac{3\pi \theta c_o D_L \rho_L a_g}{\beta^2}$$ (78)

As contaminant adsorption nears completion, the total mass adsorbed approaches the product of the maximum surface contaminant adsorption level σ_w (mass per unit area) and the total internal surface area. Hence

$$M = \frac{8 \pi \theta \sigma_w a_g^3}{3 \beta r_{min}} \tag{79}$$

and the immobile solution for $\dot{M}/M$ becomes

$$\frac{\dot{M}}{M} = \frac{9 c_o D_L \rho_L r_{min}}{8 \beta \sigma_w a_g^2} = \frac{\dot{R}_4}{a_g^2} \tag{80}$$

where

$$\dot{R}_4 = \frac{9 c_o D_L \rho_L r_{min}}{8 \beta \sigma_w} \tag{81}$$

and the coupled mobile/immobile solution is developed as described in Section VII

$$\frac{\dot{M}}{M} = (\dot{R}_3^2 \dot{R}_4)^{1/3} \tag{82}$$

where the viscosity μ in $\dot{R}_3$ reflects the properties of the liquid in the saturated medium.

One feature of the immobile solution is immediately obvious: $\dot{M}/M$ scales as $1/a_g^2$ instead of $1/a_g$ as determined for the coupled reaction/diffusive systems appropriate to combustion applications. This occurs because the late time concentration gradient within the grain is c_o/a_g and introduces an additional $1/a_g$ to the scaling relation. It is emphasized that Eq. (80) is valid only at late time as the contaminant adsorption reaches the total mass adsorption limit. At early time the integral for $\dot{M}$ is dominated by the smallest trees, the corresponding concentration gradient is much greater than c_o/a_g and $\dot{M}$ is r_{mg}/r_{min} greater than Eq. (80). The early time solution then scales as $1/a_g$ but represents the adsorption rate only at extremely low fractions of the total mass adsorption limit. This clearly indicates that a complete immobile model for this process will involve a numerical subroutine rather than a simple analytic expression. While such a model is quite tractable and would be coupled to the mobile solution as previously described, it is beyond the scope of the current study.

VIII.3 Contaminant Adsorption in Unsaturated Media

Consider a contaminated gas in a completely unsaturated medium. The contaminant will diffuse into and deposit onto the walls of the pores in exactly the same way as described for the saturated case. Within the approximation that the kinetics of the adsorption are fast with respect to the diffusion, the immobile solution is given by Eq. (80) with the gas density ρ_g replacing the liquid density ρ_L and the gas phase contaminant diffusion coefficient D_g replacing the liquid phase contaminant diffusion coefficient D_L. The immobile solution is written as

$$\frac{\dot{M}}{M} = \frac{\dot{R}_S}{a_g^2} \tag{83}$$

where

$$\dot{R}_S = \frac{9\, c_o\, D_g\, \rho_g\, r_{min}}{8\, \beta\, \sigma_w} \tag{84}$$

and the coupled mobile/immobile solution is

$$\frac{\dot{M}}{M} = (\dot{R}_3^2\, \dot{R}_S)^{1/3} \tag{85}$$

where the viscosity μ in $\dot{R}_3$ now reflects the properties of the gas in the unsaturated medium.

It is again emphasized that Eq. (85) is valid only at late time as the contaminant adsorption reaches the total mass adsorption limit and, just as in the saturated case, a complete model for this time dependent process will involve a numerical subroutine rather than a simple analytic expression. However, the analytic form of the solution appropriate to late time offers a relatively simple expression to couple into the Ground Water Simulation codes for the purpose of testing this method of coupling the mobile and immobile regions.

IX. SUMMARY

The pore tree model has been extended to describe the permeable pore structure which characterizes the subsurface transport of gas and water in soil, the dispersion of contaminants, and the in-situ remediation of contaminated sites. The random nature of the pore structure, which formed the basis of the statistical derivation of the pore tree, is applied to porous soil and sand. The interconnectivity of the pore structure is obtained via a statistical determination of the "branches" that are common to several trees to allow convection and bulk diffusion through the large scale (mobile) structure in addition to diffusion and coupled chemical reactions within the smaller scale (immobile) structure. The statistical analysis reported above has determined that the probability of pore interconnectivity extends across the entire pore size range, with a slight increase in the probability accompanying a decreasing pore size. While permeability is dominated by the largest pores, it is also important to establish the level of convection and diffusion that is occurring at the intermediate scales in order to accurately relate large scale bulk transport, intermediate scale convection, small scale diffusion and coupled chemical reactions.

The permeability across a given plane is limited by the largest pores that are interconnected in that plane. The statistical analysis has determined that approximately one quarter of one percent of all large pores are interconnected. This establishes a very coarse grid for the permeability which leads to measurement scale size errors. The extended pore tree model has successfully explained the measurement errors in the permeability of soil due to the measurement scale size (Shouse, et.al., 1994) which has indirectly confirmed the low probability of the interconnectivity.

The bulk gaseous diffusivity across a given plane is shown to be limited by the interconnectivity of the smaller branches outside of that plane. These small pores may be saturated, resulting in a strong dependence of the diffusivity on the radius of the saturated pore. A comparison of the present theory to the diffusivity data of Washington et. al., (1994) suggests a saturation radius of 30 μm. While the excellent agreement with the data does substantiate the present theory, the diffusivity in partially saturated soil is very sensitive to an unknown saturation radius. If bulk diffusivities are to be correlated with field data, such measurements should attempt to measure the saturation radius.

The permeability and the bulk diffusivity have tested two extreme limits of the pore structure and pore interconnectivity concepts. Permeability is limited by the in plane interconnectivity (Fig. 2a) and bulk gaseous diffusion is limited by the out of plane (Fig. 2b) interconnectivity. Permeability is limited by the large pore interconnectivity and bulk diffusion is limited by the interconnectivity of the smaller pores. The apparent success of these concepts over a very broad pore size range suggests that the extended pore tree model may be used to develop the subscale convection necessary to couple the mobile and immobile regions.

Since hydrodynamic dispersion is generated by the fluid velocity differences between the smaller, convection dominated pores (Garabedian et al., 1991), determination of the hydrodynamic dispersion in a homogeneous field has been used (Simons, 1996b) to test the pore interconnectivity/pore structure concepts. Data of Elrich, et al., (1966), as reported by Brusseau and Rao (1989), support the current theory of hydrodynamic dispersion. While the

long "tail" of the concentration profile is generally attributed to nonequilibrium, the current pore structure model attributes it to the wide pore size distribution occurring in soil. The narrow pore size distributions occurring in laboratory "soil" will yield a much narrower concentration profile, i.e., less hydrodynamic dispersion. Future research will be directed toward 1), evaluating the hydrodynamic dispersion as a function of pore size range in the soil sample and 2), using this analytic pore structure/ pore transport model to help derive an analytic expression for hydrodynamic dispersion that replaces the Fickian process in the transport equations.

Analysis of the permeability, bulk diffusivity, and hydrodynamic dispersion has utilized the interconnectivity of the pores to determine the distribution of the convection velocity with pore size. This analysis suggests the existence of a permeable sub-range in the pore structure which does not contribute significantly to the bulk permeability but in which convection dominates diffusion. It is the balance of the sub-scale convection with the small scale diffusion that will control contaminant transport and in-situ remediation. The size distribution of the pores and grains, and the variations in fluid velocity within and between pores of different sizes is critical to interfacing the transport processes. A methodology has been developed to couple subscale diffusion, convection and chemical reactions to the macroscopic transport in order to accurately describe contaminant transport and in-situ remediation in Ground Water Simulation codes. The fundamental approach to this application was described in Section VII and two specific examples appropriate to limiting cases of subscale transport were developed in Section VIII. Future research will be directed toward developing a library of models for chemical/diffusive processes in the immobile region such that they may be coupled to the mobile region via the technique derived above. Such models will provide Ground Water Simulation Codes with physically realistic submodels for contaminant transport and remediation studies that can be used to scale data from the laboratory to the field and from one field site to another.

X. REFERENCES

Brusseau, M.L. and Rao, P.S.C. (1989), "Sorption Nonideality During Organic Contaminant Transport in Porous Media," Critical Reviews in Environmental Control, 19, 33-99.

Dullien, F.A.L. (1979), *Porous Media Fluid Transport and Pore Structure,* Academic Press, pp 160-161.

Elrich, D.E., Erh, K.T., and Krupp, H.K. (1966), "Applications of Miscible Displacement Techniques to Soils," Water Resour. Res. 2, 717.

Garabedian, S.P., LeBlanc, D.R., Gelhar, L.W. and Celia, M.A. (1991), "Large-Scale Natural Gradient Test in Sand and Gravel," Water Resources Research, 27, 911-924.

Gavalas, G.R. (1980), "A Random Capillary Model with Application to Char Gasification at Chemically Controlled Rates," AIChE J., 26, 577.

Gavalas, G.R. (1981), "An Analysis of Char Combustion Including the Effect of Pore Enlargement," Comb. Sci. Tech., 24, 197.

Kothandaraman, G. and Simons, G.A. (1984), "Evolution of the Pore Structure in PSOC 140 Lignite During Pyrolysis," The Combustion Institute, Twentieth Symposium (International) on Combustion, Ann Arbor, MI.

Lewis, P.F. and Simons, G.A. (1979), "Char Gasification: Part II. Oxidation Results," Comb. Sci. Tech., 20, 3 & 4, 117-124.

Shouse, P.J., Ellsworth, T.R. and Jobes, J.A. (1994), "Steady-State Infiltration as a Function of Measurement Scale," Soil Science, 157, 3, 129-136.

Simons, G.A. and Finson, M.L. (1979), "The Structure of Coal Char: Part I. Pore Branching," Comb. Sci. Tech., 19, 5 & 6, 217-226.

Simons, G.A. (1979a), "The Structure of Coal Char: Part II. Pore Combination," Comb. Sci. Tech., 19, 5 & 6, 227-235.

Simons, G.A. (1979b), "Char Gasification: Part I. Transport Model," Comb. Sci. Tech., 20, 3 & 4, 107-116.

Simons, G.A. and Rawlins, W.T. (1980), "The Reaction of SO_2 and H_2S with Porous Calcined Limestone," Ind. & Eng. Chem., Process Des. & Dev., 19, 565-572.

Simons, G.A. (1982), "The Pore Tree Structure of Porous Char," The Combustion Institute, Nineteenth Symposium (International) on Combustion, Haifa, Israel.

Simons, G.A. (1983a), "The Role of Pore Structure In Coal Pyrolysis and Gasification," (Invited Survey Article) Progress in Energy and Combustion Science, 9, 269.

Simons, G.A. (1983b), "Coal Pyrolysis I. Pore Evolution Theory," Comb. and Flame, 53, 83-92.

Simons, G.A. (1984), "Coal Pyrolysis II. Species Transport Theory," Comb. and Flame, 55, 181-194.

Simons, G.A., Garman, A.R., and Boni, A.A. (1984), "High Pressure Sulfur Sorption by Limestone," Paper No. 33, Eastern Section of the Combustion Institute, Fall Technical Meeting, Clearwater Beach, FL.

Simons, G.A., Ham, D.O., and Moniz, G.A. (1986), "Catalytic Cracking of Aromatic Hydrocarbons", Physical Sciences Inc. PSI-385/TR-552, DOE/MC/21385-2021.

Simons, G.A. and Garman, A.R. (1986), "Small Pore Closure and the Deactivation of the Limestone Sulfation Reaction," AIChE J., 32, 1491.

Simons, G.A., Garman, A.R., and Boni, A.A. (1987), "The Kinetic Rate of SO_2 Sorption by CaO," AIChE J., 33, 211.

Simons, G.A. (1988), "Parameters Limiting Sulfation by CaO," AIChE J., <u>34</u>, 167.

Simons, G.A. (1991), "Predictions of CMA Utilization for In-Situ SO_2 Removal in Utility Boilers," International Symposium on Calcium Magnesium Acetate (CMA), Northeastern University, Boston, MA, May 14-16. Also: Resources, Conservation and Recycling, <u>7</u>, 161-170, 1992.

Simons, G.A., Parker, T.E., Moore, J.W., Senior, C.A., and Levendis, Y.A. (1992), "Combined NO_x/SO_x Control Using a Single Liquid Injection System," Physical Sciences Inc., TR-1169.

Simons, G.A., (1996a), "Extension of the "Pore tree" Model to Describe Transport in Soil," Ground Water,<u>34</u>, 4, July-August, 683-690.

Simons, G.A. (1996b), "Application of the "Pore tree" Model to Describe Hydrodynamic Dispersion," Submitted for publication, Ground Water.

Washington, J.W.; Rose, A.W.; Ciolkosz, E.J.; and Dobos, R.R. (1994), "Gaseous Diffusion and Permeability in Four Soil Profiles in Central Pennsylvania," Soil Science, <u>157</u>, 2, 65-76.

XI. NOMENCLATURE

A	arbitrary cross sectional area
A_θ	area within A that is connected
a	radius of sphere in a porous medium
a_{max}	maximum value of a in which pore structure is self similar
a_g	radius of arbitrary "grain" of soil
c	species mass fraction (ρ_c/ρ_g)
$\bar{c}$	mean species concentration
D_h	hydrodynamic dispersion coefficient
D_g	continuum gas phase diffusion coefficient
D_L	contaminant diffusion coefficient in the liquid
D_{bulk}	gas diffusion coefficient in partially saturated porous media
D_{limit}	gas diffusion coefficient in fully connected porous media
$f(r_p)$	number of pores per unit volume of radius r_p
$\bar{g}(r_p)$	number of pores per unit area of radius r_p
$\bar{G}_t$	number of pores in tree r_t and in plane A of radius r_p
$\bar{I}(r_p)$	common branch distribution function $\bar{I} = \bar{g}\,P_I$
k	permeability
k_g	permeability of grain a_g
K_o	constant relating the pore length to the radius
l_p	length of a pore of radius r_p
l_t	length of a tree trunk of radius r_t
$\dot{M}_p(r_p)$	diffusive mass flux in pore of radius r_p
$\dot{M}_\infty(r_p)$	diffusive mass flux in tree r_p limited by interconnectivity
$\dot{M}/M$	mobile/immobile rate (1/t)
N_t	number of pores in tree r_t of radius r_p
$n(x)$	number of branches at location x
$P_I(r_p)$	probability of interconnectivity
p	gas or liquid pressure
$\dot{Q}$	convective volume flow rate across cross sectional area A
$\dot{Q}_p(r_p)$	convective volume flow rate in pore of radius r_p
$\dot{Q}_\infty(r_p)$	convective volume flow rate in tree r_p limited by interconnectivity
$\dot{R}_j$	mobile/immobile rate constants
r_p	radius of a pore
r_t	radius of trunk of tree r_t
r_c	radius of penetration of contaminant adsorption
r_{mg}	maximum pore radius in grain a_g
r_{sat}	radius of largest pore that is saturated
r_1	largest pore corresponding to $v_m(r_1)$
r_2	smallest pore corresponding to $v_m(r_1)$

37

s_p	specific internal surface area (m^2/g)
$S_t(r_t)$	surface area of pore tree with trunk radius r_t
t	time
$V_t(r_t)$	volume of pore tree with trunk radius r_t
$v_p(r_p)$	velocity associated with $\dot{Q}_p(r_p)$
$v_m(r_p)$	mean value of $v_p(r_p)$ in interconnected pore space
$\bar{v}$	mean velocity across area θA
x	axial distance in pore, spatial coordinate
x_c	axial penetration of contaminant adsorption

Greek

β	$\ln (r_{max} / r_{min})$
η	dimensionless coordinate: Eq (56)
θ	total porosity of the porous medium
θ_a	unsaturated or "air filled" porosity of the medium
λ	hydrodynamic dispersivity
μ	viscosity of permeate
ρ_c	density of gas phase species c
ρ_g	total density of gas phase
ρ_s	density of the solid matrix
ρ_L	density of the liquid
σ_w	maximum surface contaminant adsorption level (mass per unit area)
τ	time constant for complete contaminant adsorption

Subscripts

p	pore
t	tree whose trunk reaches outer edge of medium
s	tree whose trunk is in arbitrary plane
min	minimum size
max	maximum size